Journal of Solid State Chemistry **153,** 237–247 (2000)
doi:10.1006/jssc.2000.8747, available online at http://www.idealibrary.com on IDEAL®

Synthesis and Phase Characterization of a Solid Solution Series between β-$Fe_2(PO_4)O$ and $Fe_4(PO_4)_3(OH)_3$

P. Schmid-Beurmann

Institut für Geowissenschaften, Christian Albrechts Universität Kiel, Ohlshausenstrasse 40, D-24098 Kiel, Germany

Received December 28, 1999; in revised form April 17, 2000; accepted 20, 2000; published online July 7, 2000

An intermediate solid solution series was synthesized in the quaternary system FeO–Fe_2O_3–P_2O_5–H_2O between the compositions of $Fe_2(PO_4)O$ and $Fe_4(PO_4)_3(OH)_3$ hydrothermally at 586°C and 0.3 GPa. Quantitative XRPD studies in combination with chemical bulk analysis reveal that under these conditions an intermediate solid solution series is formed in the above-mentioned quarternary system. It was found to range between $0.18 \leq x \leq 0.60$ according to a stoichiometry of $Fe^{3+}_{4-x}Fe^{2+}_{3x}(PO_4)_3(OH)_{3-3x}O_{3x}$. In the range of $0.02 \leq x \leq 0.18$ a two-phase field exists under these conditions between the limiting member of the intermediate solid solution and $Fe_4(PO_4)_3(OH)_3$ with a small miscibility region in direction of $Fe_2(PO_4)O$. On the other hand, the hypothetical end-member $Fe_2(PO_4)O$ could not be synthesized under these conditions. Using standard X-ray powder diffraction in combination with the Rietveld method, the members of the solid solution were found to crystallize analogously to β-$Fe_2(PO_4)O$ in the tetragonal space group $I4_1/amd$. The solid solutions are characterized by a disordered distribution of Fe^{2+}, Fe^{3+}, and vacancies over the single octahedrally coordinated *Me* (8*f*) site.

Key Words: **Fe-phosphates; hydrothermal method; Rietveld method; Lazulite-type.**

INTRODUCTION

Synthetic iron phosphates are known from a series of patents (1,2) as catalysts for the oxidative dehydrogenation of isobutyric acid to methacrylic acid. This is a step in the process of the synthesis of methylmethachrylate in which the redox pair Fe^{2+}/Fe^{3+} plays a prominent role (3). The catalysts actually used are mixtures of anhydrous iron phosphates, which change their composition and their state of oxidation under the conditions of (4). In catalytic studies of different iron hydroxy phosphates (3,5) it was reported that synthetic barbosalite and synthetic lipscombite, both $Fe^{2+}Fe^{3+}_2(OH)_2(PO_4)_2$, as well as $Fe_{4.24}(PO_4)_3(OH)_{2.28}O_{0.72}$ and $Fe_5(PO_4)_3O_3$ change their composition during the catalytic process resulting in three members of a possible solid solution series with the formula $Fe^{3+}_{4-x}Fe^{2+}_{3x}(PO_4)_3(OH)_{3-3x}O_{3x}$ between β-$Fe^{2+}Fe^{3+}(PO_4)O$ and $Fe^{3+}_4(OH)_3(PO_4)_3$ (Fig. 1). In order to clarify the extent of this solid solution series and to characterize its crystal chemical properties an investigation was started aiming at the synthesis and the characterization of the solid solution series. According to (3), these phases are supposed to contain variable amounts of hydroxyl ions. Experiments using the hydrothermal method were performed.

PREVIOUS WORK

β-$Fe_2(PO_4)O$ was prepared the first time by evaporating an aqueous solution of $Fe(NO_3)_3$ and $(NH_4)_2HPO_4$ or H_3PO_4 at temperatures up to 400°C and performing subsequent reduction in an H_2–H_2O gas atmosphere at 450°C at ambient pressures (6). The compound undergoes two phase transitions according to the sequence

$$\beta\ (\text{mcl}) \Rightarrow 142^\circ\text{C} \Rightarrow \beta\ (\text{tet}) \Rightarrow 700\text{–}800^\circ\text{C} \Rightarrow \alpha.$$

According to (7), the β-form is metastable with respect to α-$Fe_2(PO_4)O$ as it transforms irreversibly to the latter phase.

The monoclinic compound $Fe_4(OH)_3(PO_4)_3$ was first synthesized in (8) and (9) independently using the hydrothermal method at temperatures of about 400°C. Despite the different lattice symmetries the structures of the title compounds are strongly related (Figs. 2a and 2b). This structure type can be regarded as built up of layers of infinite chains formed by face-sharing oxygen octahedra. Between alternating layers the chains are perpendicular to each other and they are interconnected via PO_4 tetrahedra and common oxygen or hydroxyl ions. In β-$Fe_2(PO_4)O$ the face-sharing octahedra are completely occupied by Fe^{2+} and Fe^{3+} ions. At room temperature and using a standard X-ray source the structure was found to be tetragonal ($I4_1/amd$) with all iron ions distributed over a single site (8*f*) (7). Using powder diffraction (10) in combination with synchroton radiation a monoclinic distortion of the structure with space group $I2/a$ could be detected with two different Fe sites (4*b* and 4*c*).

0022-4596/00 $35.00

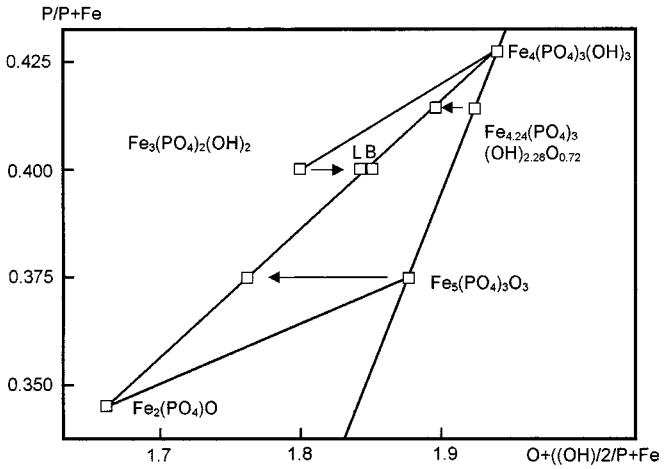

FIG. 1. Ternary section through the system $FeO–Fe_2O_3–P_2O_5–H_2O$ with the representing points and reaction paths of the iron phosphates used in catalytic experiments (4). B, L: barbosalite und lipscombite after catalysis.

TABLE 1
Conditions for X-Ray Powder Data Collection for Rietveld Refinement

Diffractometer	Siemens D 5000 ($\theta/2\theta$)
Radiation	Cu$K\alpha$
Radius	250 mm
Monochromator	Secondary
Current/voltage	25 mA/40 kV
2θ-range (°)	17–70
Step size (°)	0.01
Measuring time/step	7–8 s
Mode	Continuous scan
Soller slits	Primary and secondary
Prim. divergency slit	Fixed (0.5°)[a]
Sec. divergency slit	1.0
Detector slit	0.6 mm
Sample rotation	15 rounds s^{-1}

[a]Aperture angel.

As bond valency calculations gave almost the same charge for the two Fe species an attribution of ferrous and ferric irons to these different sites cannot be justified (10). At low temperatures ferrous and ferric ions are coupled ferromagnetically in the octahedral chains but antiferromagnetically between the chains. At higher temperatures a fast intervalence charge transfer appears between neighboring Fe^{2+} and Fe^{3+} ions resulting in ^{57}Fe Mößbauer spectra showing one quadrupole dublet for $Fe^{2.5+}$ (6). In $Fe_4(OH)_3(PO_4)_3$ pairs of Fe^{3+} ions are formed which are separated by an empty octahedron. Below 150 K these Fe^{3+} pairs are antiferromagnetically ordered.

EXPERIMENTAL PROCEDURE

Synthesis

In order to synthesize members of the solid solution between $Fe_2(PO_4)O$ and $Fe_4(PO_4)_3(OH)_3$ (which are further denoted as $Fe_2(PO_4)O_{ss}$) samples with the starting bulk compositions of Table 2 according to the stoichiometry of $Fe^{3+}_{4-x}Fe^{2+}_{3x}(PO_4)_3(OH)_{3-3x}O_{3x}$ ($= x3Fe_2(PO_4)O + (1-x)Fe_4(PO_4)_3(OH)_3$) were used in combination with standard hydrothermal techniques. As starting materials, Fe (Merck No. 819 p.a.), Fe_2O_3 (Merck No. 3924), $FePO_4$ (berlinite form), and deionized H_2O were used according to the formal reaction equation

$$x\mathrm{Fe} + x\mathrm{Fe_2O_3} + (4-x)\mathrm{FePO_4} + (3-3x)/2\mathrm{H_2O} \Rightarrow \mathrm{Fe}^{3+}_{4-x}\mathrm{Fe}^{2+}_{3x}(\mathrm{PO_4})_3(\mathrm{OH})_{3-3x}\mathrm{O}_{3x}. \quad [1]$$

$FePO_4$ was synthesized from pelletized stoichiometric mixtures of Fe_2O_3 and $(NH_4)H_2PO_4$ (Fluka No. 09709) by successive heatings in an open platinum crucible between 350°C and 1000°C. After a regrainment the product was again pelletized and heated in an open silica tube at 1000°C for 3 days. The phase characterization using X-ray powder diffraction revealed single-phase $FePO_4$ with the berlinite (α-$AlPO_4$) structure.

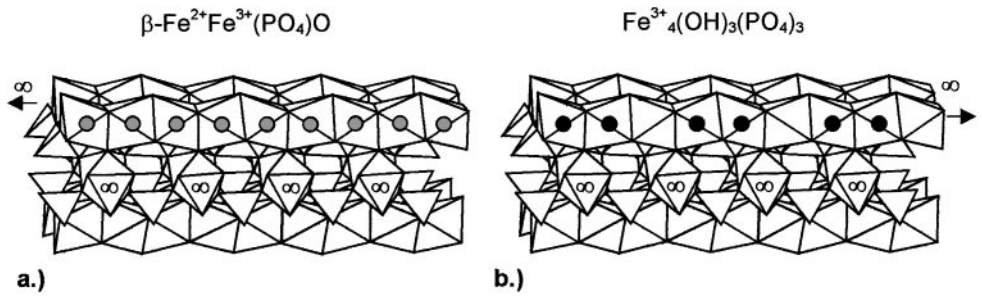

FIG. 2. Iron distribution in (a) β-$Fe^{2+}Fe^{3+}(PO_4)O$ (10) and (b) $Fe^{3+}_4(OH)_3(PO_4)_3$ (8,9). Black circles, Fe^{3+}; gray circles, Fe with intermediate valency. This structure type can be regarded as built up of infinite chains of face-sharing oxygen octahedra which are interconnected via PO_4 tetrahedra and common oxygen or hydroxyl ions. In β-$Fe_2(PO_4)O$ the face-sharing octahedra are fully occupied whereas in $Fe^{3+}_4(OH)_3(PO_4)_3$ pairs of Fe^{3+} ions are present which are separated by an empty octahedron (designed after Rouzies and Millet, 1993).

TABLE 2
Synthesis Experiments at 586°C and 0.3 GPa

Sample	Starting bulk composition				Phase composition of the run products
	$x_{Fe_2O_3}$[a]	x_{FeO}[a]	$x_{P_2O_5}$[a]	x_{start}[b]	
Barb-35	0.250	0.500	0.250	1.000	$Fe_2(PO_4)O_{SS}$ (84), Hem (1), Sarc (15)
Barb-138	0.286	0.444	0.270	0.824	$Fe_2(PO_4)O_{SS}$ (95), Hem (3), Sarc (2)
Barb-137	0.323	0.387	0.290	0.667	$Fe_2(PO_4)O_{SS}$ (97), Hem (3)
Barb-136	0.361	0.328	0.311	0.526	$Fe_2(PO_4)O_{SS}$ (97), Hem (3)
Barb-131	0.400	0.267	0.333	0.400	$Fe_2(PO_4)O_{SS}$ (99), Hem (1)
Barb-148	0.441	0.203	0.356	0.286	$Fe_2(PO_4)O_{SS}$ (98), Hem (2)
Barb-134	0.483	0.138	0.379	0.182	$Fe_2(PO_4)O_{SS}$ (99), Hem (1)
Barb-133	0.526	0.070	0.404	0.087	$Fe_2(PO_4)O_{SS}$ (57), $Fe_4(PO_4)_3(OH)_3$ (43)
Barb-139	0.571	0.000	0.429	0.000	$Fe_4(PO_4)_3(OH)_3$ (100)

Note. Starting materials: Fe, Fe_2O_3, $FePO_4$, and H_2O. [a]Molar ratios in the ternary system FeO–Fe_2O_3–P_2O_5. [b]Compositional parameter x_{start} according to the formula of $Fe^{3+}_{4-x}Fe^{2+}_{3x}(PO_4)_3(OH)_{3-3x}O_{3x}$. Abbreviations: $Fe_2(PO_4)O_{ss}$, member of the solid solution series between $Fe_2(PO_4)O$ and $Fe_4(PO_4)_3(OH)_3$; Hem, hematite, α-Fe_2O_3; Sarc, sarcopside ($Fe_3(PO_4)_2$).

The starting compounds for the synthesis of the $Fe_2(PO_4)O_{ss}$ solid solutions were weighed in the appropriate proportions and homogenized in a mortar. About 450 mg of sample was sealed into Au tubes with an outer diameter of 5 mm, a wall thickness of 0.1 mm, and a length of 40 mm together with 25 µl of distilled water. The experiments were carried out in a conventional hydrothermal apparatus with horizontally arranged Tuttle-type cold-seal bombs at a temperature of $T = 586°C$ and at a pressure of $P = 0.3$ GPa. The temperature was controlled using Ni–CrNi thermocouples. The overall uncertainty in temperature was estimated to be less than $\pm 5°C$. The pressure was measured with a Heise gauge, and as it could not be read better than ± 2.5 MPa, this was considered to be the uncertainty in pressure. An experiment was ended by switching off the power. The autoclaves were then cooled in a cold air stream. Room temperature was attained within 1/2 hour. The experiment durations were 24–25 hours.

Chemical Bulk Analysis

Chemical bulk analyses were performed on 80 to 230 mg of material. Before analysis the samples were evacuated in a desiccator at room temperature overnight in order to withdraw adsorbed H_2O. Any heat treatment was avoided at this stage of preparation because of possible oxidation, reduction, or decomposition of the compounds. Atomic absorption spectrophotometry was used to determine Fe^{tot}. The phosphorus content was measured by colorometry. The Ungethüm method (11) has been applied for the determination of Fe^{2+}. The thermal analyses have been obtained with a NIETZSCH STA 449C instrument, under nitrogen and in the temperature range from 20–900°C.

X-Ray Powder Diffraction

X-ray powder diffractions for qualitative and quantitative phase analysis using the Rietveld method were recorded using a SIEMENS D5000 powder diffractometer with Cu$K\alpha$ radiation, a secondary graphite-(001) monochromator, and the conditions of Table 1. The samples were ground in an agate mortar and 200–300 mg of the powder was filled into aluminum sample holders, smoothed by a microscopy glass substrate giving layers with a diameter of 2.5 cm and 0.1 mm thickness, and then fixed in the sample holder of the instrument.

RESULTS

Characterization of the $Fe_2(PO_4)O_{ss}$ Solid Solution Series

The reaction products of the hydrothermal experiments consisted of fine grained powders. Their color changed with increasing content of the $Fe_2(PO_4)O$ component from light greenish to black. The members of the $Fe_2(PO_4)O_{ss}$ solid solution series were present as rounded isometric crystals showing faces (Fig. 3) and diameters up to 10 µm. Sarcopside, $Fe_3(PO_4)_2$, when present in the samples, could easily be recognized as it forms yellowish transparent crystals.

Synthesis Experiments

The compositions of the anhydrous starting materials of the synthesis runs are given as molar fractions of the oxides FeO, P_2O_5, and Fe_2O_3 and as the compositional parameter x according to the bulk chemical formula $Fe^{3+}_{4-x}Fe^{2+}_{3x}(PO_4)_3(OH)_{3-3x}O_{3x}$ together with the results of the quantitative phase analysis in Table 2. The weight

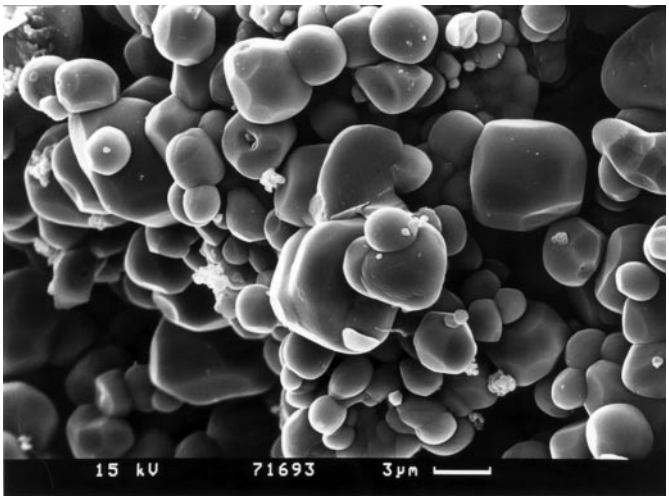

FIG. 3. Scanning electron microscopic photograph of a hydrothermally synthesized member of the $Fe_2(PO_4)O_{ss}$ solid solution series.

portions of the present phases were determined using multiphase Rietveld refinement of the X-ray powder diffractograms. The weight percentages of the detected phases are given in parentheses.

The chemical bulk analysis of eight samples prepared at 586°C can be taken from Table 3. In Table 4 the chemical formulas of the members of the $Fe_2(PO_4)O_{ss}$ solid solutions series present in these samples are given together with their lattice constants derived from Rietveld refinement. These compositions were calculated from the chemical bulk analysis of Table 3 and corrected by the weight portions of the phases besides $Fe_2(PO_4)O_{ss}$ from column 5 of Table 2. The chemical formulas are normalized to three phosphorus atoms according to the ideal formula of $Fe_{4-x}^{3+}Fe_{3x}^{2+}(PO_4)_3(OH)_{3-3x}O_{3x}$. The compositional parameter x (column 3, Table 4) was determined by projecting the corresponding data points in the anhydrous system $FeO–Fe_2O_3–P_2O_5$ (Fig. 5) onto the pseudobinary tieline between the $Fe_2(PO_4)O$ and the $Fe_4(PO_4)_3(OH)_3$ compositions. This value can also be used as a measure of the molar portion of the $Fe_6(PO_4)_3O_3$ component in the solid solutions.

The full results of the Rietveld refinement of the $Fe_2(PO_4)O_{ss}$ phases starting with the structural data for tetragonal β-Fe_2PO_4O taken from (7) are presented in Table 5.

DISCUSSION

Phase Compositions of the Run Products

Figure 4 shows the powder diffractions of the samples from Table 2. In these diffractograms the reflections of (1) monoclinic $Fe_4(PO_4)_3(OH)_3$, (2) members of a tetragonal solid solution series (denoted as $Fe_2(PO_4)O_{ss}$) intermediate between the compositions of $Fe_4(PO_4)_3(OH)_3$ and $Fe_2(PO_4)O$, as well as (3) α-Fe_2O_3 (hematite) and $Fe_3(PO_4)_2$ (sarcopside) could be identified.

Sample Barb-139 with a starting composition of $x_{start} = 1.0$ was found to consist of pure monoclinic $Fe_4(PO_4)_3(OH)_3$. With increasing x_{start} the reflections of this phase disappear from the diffractograms (Barb-139 through Barb-134) and are replaced by those of tetragonal $Fe_2(PO_4)O_{ss}$ (Barb-134). Sample Barb-133 was found to be composed of both phases and is therefore compositionally located in the two-phase region between the limiting member of the intermediate $Fe_2(PO_4)O_{ss}$ solid solution series and $Fe_4(PO_4)_3(OH)_3$. At intermediate contents of x_{start} (samples Barb-134 to Barb-138) the diffractions reveal the presence of prevailing $Fe_2(PO_4)O_{ss}$ with small admixtures of hematite. The variation of the d values of the solid solutions with composition can directly be observed from the variation of the 2θ values of the (004) and (121) reflections for example. Nearly pure $Fe_2(PO_4)O_{ss}$ with only small admixtures of hematite was found to be present in sample Barb-131.

At high x_{start} from 0.82 up to 1.00 of the starting mixture the $Fe_2(PO_4)O–Fe_4(PO_4)_3(OH)_3$ section becomes pseudobinary as sample Barb-35 with the bulk starting composition of $Fe_2(PO_4)O$ ($x_{start} = 1.0$) was found to consist of α-Fe_2O_3 (hematite), $Fe_3(PO_4)_2$ (sarcopside), and $Fe_2(PO_4)O_{ss}$. Pure β-$Fe_2(PO_4)O$ could therefore not be synthesized under these conditions.

In Fig. 5 the phase compositions of the $Fe_2(PO_4)O_{ss}$ phases which were derived from the results of the quantitat-

TABLE 3
Chemical Bulk Analyses

Sample	Barb-138 (wt.%)	Barb-137 (wt.%)	Barb-136 (wt.%)	Barb-131 (wt.%)	Barb-148 (wt.%)	Barb-134 (wt.%)	Barb-133 (wt.%)	Barb-139 (wt. %)
P_2O_5	32.87	32.99	34.08	36.09	35.06	36.93	36.99	37.51
Fe_2O_3	45.32	44.98	47.95	49.74	49.74	52.7	53.05	55.84
FeO	20.94	18.25	15.16	12.46	11.18	6.63	4.56	1.25
H_2O	1.65	2.55	3.15	3.32	4.16	4.07	4.53	4.70
Total	100.78	98.77	100.34	101.61	100.14	100.33	99.13	99.30

Analyst: J.-M. Speetjens.

TABLE 4
Chemical Composition and Lattice Parameters

Sample	Formula of $Fe_2(PO_4)O_{ss}$ member[a]	x_{exp}[b]	Lattice constants of $Fe_2(PO_4)O$ss member		
			a [Å]	c [Å]	V [Å^3]
	Tetragonal Phases				
Barb-138	$Fe^{3+}_{3.52}Fe^{2+}_{1.83}(PO_4)_3(OH)_{1.21}O_{2.00}$	0.60	5.2965(2)	12.6841(6)	355.83(3)
Barb-137	$Fe^{3+}_{3.42}Fe^{2+}_{1.64}(PO_4)_3(OH)_{1.83}O_{1.35}$	0.55	5.2718(2)	12.7817(7)	355.23(3)
Barb-136	$Fe^{3+}_{3.56}Fe^{2+}_{1.32}(PO_4)_3(OH)_{2.18}O_{1.06}$	0.44	5.2536(3)	12.8325(9)	354.17(5)
Barb-131	$Fe^{3+}_{3.60}Fe^{2+}_{1.02}(PO_4)_3(OH)_{2.17}O_{0.84}$	0.35	5.2427(3)	12.852(1)	353.24(5)
Barb-148	$Fe^{3+}_{3.68}Fe^{2+}_{0.94}(PO_4)_3(OH)_{2.80}O_{0.56}$	0.32	5.2273(7)	12.891(3)	352.2(1)
Barb-134	$Fe^{3+}_{3.76}Fe^{2+}_{0.53}(PO_4)_3(OH)_{2.60}O_{0.37}$	0.18	5.2167(4)	12.909(1)	351.30(6)
Barb-133	$Fe^{3+}_{3.65}Fe^{2+}_{0.66}(PO_4)_3(OH)_{2.81}O_{0.22}$	0.23	5.2158(4)	12.916(1)	351.39(6)
	Monoclinic Phase				
Barb-139	$Fe^{3+}_{3.97}Fe^{2+}_{0.10}(PO_4)_3(OH)_{2.96}O_{0.07}$	0.03	a 19.581(1) b 12.891(3)	c 7.4359(3) β 102.16(1)	mcl. 1051.3(1)[c]

[a]Calculated from the chemical bulk composition (Table 3) and the weight portions of phases others than $Fe_2(PO_4)O_{ss}$ (Table 2). [b]Compositional parameter x ($Fe^{3+}_{4-x}Fe^{2+}_{3x}(PO_4)_3(OH)_{3-3x}O_{3x}$) determined by projecting the representing points of the compositions (column 2) in the anhydrous system $FeO–Fe_2O_3–P_2O_5$ onto the pseudobinary tieline between $Fe_2(PO_4)O$ and $Fe_4(PO_4)_3(OH)_3$. [c]In Fig. 8 $V/3$ is presented for better comparison to the volumes of the members of the $Fe_2(PO_4)O_{ss}$ solid solution series.

ive phase analysis (Table 2) and the chemical bulk analysis (Table 3) are shown as projections on to the ternary system $FeO–P_2O_5–Fe_2O_3$ as crosses (+). These compositions fit onto the pseudobinary join between the $Fe_2(PO_4)O$ and the $Fe_4(PO_4)_3(OH)_3$ compositions. In Fig. 6 the result of the chemical bulk analysis concerning the water content of the samples (Table 3) within the range of the $Fe_2(PO_4)O_{ss}$ is shown as a projection onto the ternary system

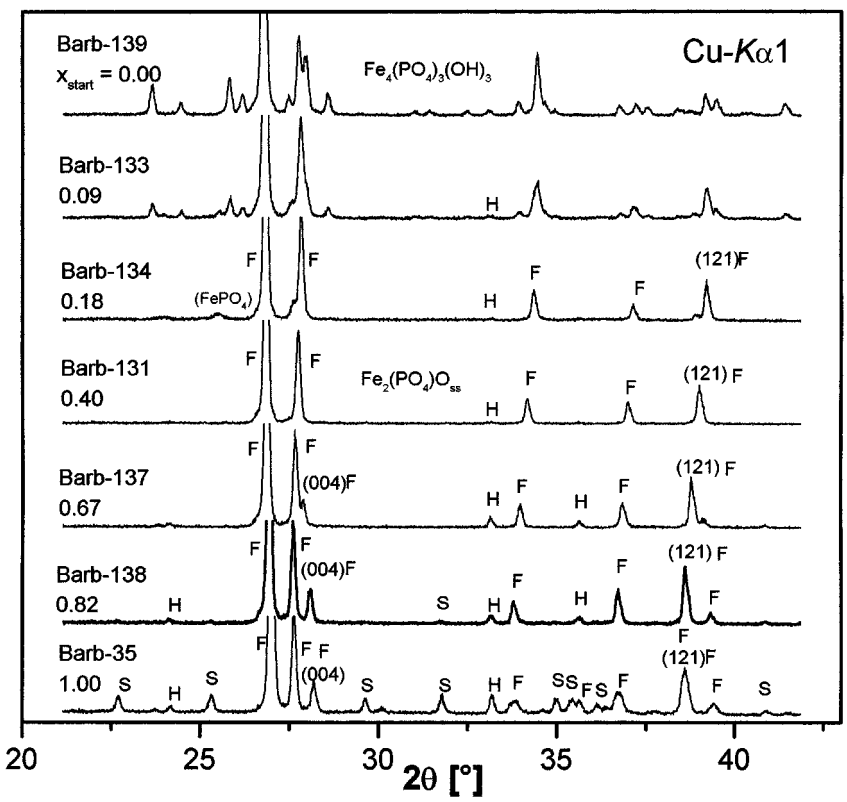

FIG. 4. Powder diffractograms of samples synthesized at 586°C (0.3 GPa) between the $Fe_2(PO_4)O$ and the $Fe_4(OH)_3(PO_4)_3$ compositions. F, $Fe_2(PO_4)O_{ss}$; H, hematite; S, Sarcopside.

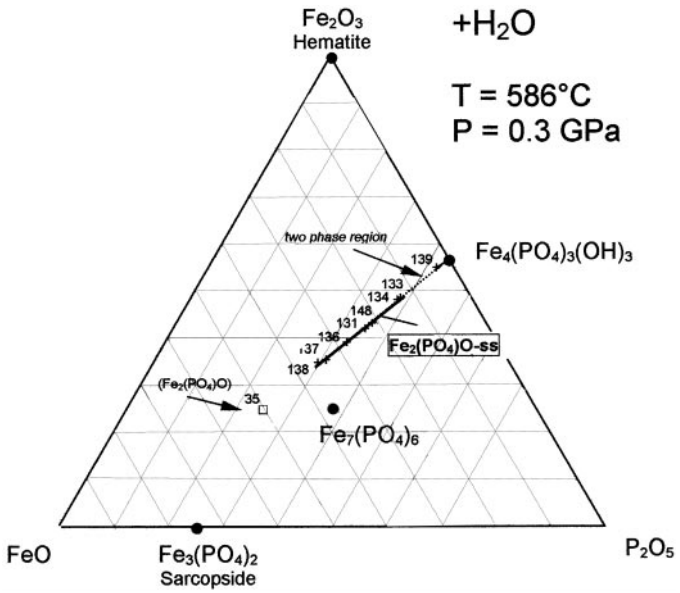

FIG. 5. Extension of the $Fe_2(PO_4)O_{ss}$ solid solution series between the $Fe_2(PO_4)O$ and $Fe_4^{3+}(OH)_3(PO_4)_3$ compositions in the system Fe_2O_3–FeO–P_2O_5–H_2O projected from the H_2O apex onto the anhydrous base at 586°C and 0.3 GPa. +, composition of members of the $Fe_2(PO_4)O_{ss}$ solid solution series according to their chemical formula (Table 4); open square, representing data point of the $Fe_2(PO_4)O$ composition.

FeO–Fe_2O_3–H_2O. With decreasing x_{exp} or increasing content of the ferric component $Fe_4(PO_4)_3(OH)_3$ the samples contain increasing amounts of water, as was expected in the case of solid solution between $Fe_4(PO_4)_3(OH)_3$ and $Fe_2(PO_4)O$. Nevertheless, a variable excess of water with respect to the ideal formula, which is represented by the straight line between the representing data points of $Fe_2(PO_4)O$ and $Fe_4(PO_4)_3(OH)_3$ in Fig. 6, is obvious. This may be due to adsorbed humidity which could not be removed by evacuating at room temperature.

According to Figs. 5 and 6 the conclusion can be drawn that in the quaternary system FeO–P_2O_5–Fe_2O_3–H_2O an incomplete and intermediate solid solution series exists between the $Fe_2(PO_4)O$ and the $Fe_4(PO_4)_3(OH)_3$ compositions. The range of this solid solution can be quantified to $0.18 < x < 0.60$. Neither the pure β-$Fe_2(PO_4)O$ phase nor the α-modification formed under the conditions of 586°C and 0.3 GPa.

It was reported (7) that hydrothermal treatment of β-$Fe_2(PO_4)O$ at 0.4 GPa and 600°C produced a hydrolysis into $Fe_3(PO_4)_2$ and Fe_2O_3 plus H_3PO_4. As nothing was reported in (7) about buffering of their sample or run durations, the absence of $Fe_2(PO_4)O_{ss}$ in their hydrothermal run products can also be explained by a reduction of a part of the ferric iron. This may occur in unbuffered experiments as the oxygen fugacity in the sample container is influenced by that of the outer pressure medium. As the bomb wall oxygen fugacity approaches that of the Ni/NiO buffer (12) a reduction of samples containing ferric iron can be expected. The extent of this reduction depends at constant temperature and pressure on the material of the autoclave, the material

TABLE 5
Structural and Cell Parameters of $Fe_2(PO_4)O_{ss}$ from the Rietveld Rrefinement in Space Group $I4_1/amd$, $Z=4$

Sample, x_{exp}[a]	Barb-35	Barb-138, 0.60	Barb-137, 0.55	Barb-136, 0.44	Barb-131, 0.35	Barb-148, 0.32	Barb-134, 0.18	Barb-133, 0.23
Fe 8*f*				$x = 0$; $y = 0$; $z = 1/2$				
SOF	0.86(3)	0.87(1)	0.83(1)	0.79(1)	0.77(1)	0.77(2)	0.70(1)	0.71(1)
P 4*a*				$x = 0$; $y = 3/4$; $z = 1/8$				
SOF	0.99(4)	0.98(1)	0.98(1)	0.98(1)	1.02(2)	1.02(1)	0.99(2)	0.98(2)
O1 16*h* *x*				$x = 0$				
y	0.498(3)	0.492(1)	0.492(1)	0.492(1)	0.504(2)	0.494(3)	0.492(2)	0.490(2)
z	0.806(1)	0.8071(4)	0.8069(4)	0.8071(5)	0.8103(7)	0.807(1)	0.8071(8)	0.8072(2)
O2 4*b*				$x = 0$; $y = 1/4$; $z = 3/8$;				
B_{over}	1.93(6)	0.85(5)	1.10(6)	1.14(5)	2.06(5)	1.87(8)	1.18(6)	0.60(5)
a	5.3053(6)	5.2965(2)	5.2718(2)	5.2536(3)	5.2427(3)	5.2273(7)	5.2167(4)	5.2158(4)
c	12.662(2)	12.6841(6)	12.7817(7)	12.8325(9)	12.852(1)	12.891(3)	12.909(1)	12.916(1)
V	355.4(3)	355.83(3)	355.23(3)	354.17(5)	353.24(5)	352.2(1)	351.30(6)	351.39(6)
w	0.0257(5)	0.0127(2)	0.0164(3)	0.0146(3)	0.0128(2)	0.0216(7)	0.0130(2)	0.0132(3)
asy	− 0.07(4)	− 0.17(4)	− 0.15(4)	− 0.06(3)	− 0.06(4)	0.04(2)	0.03(5)	0.20(5)
n_a	0.47(1)	0.62(1)	0.55(1)	0.70(1)	0.55(1)	0.87(2)	0.55(1)	0.55(1)
No. of profile points	5300	5300	5300	5300	5300	5300	5300	5300
No. of refined parameters	31	27	21	21	21	18	18	24
$R_{wp} = 100\{\sum w(y_{obs} - y_{cal})^2 \in \sum w y_{obs}^2\}^{1/2}$	22.1	17.1	18.1	17.4	17.3	22.4	19.4	16.5
$R_p = 100\{\sum\lvert y_{obs} - y_{cal}\rvert/\sum\lvert y_{obs}\rvert\}$	16.5	12.3	13.2	12.6	12.9	17.3	14.2	12.2
$R_{exp} = 100\{(N - P)/\sum w y_{obs}^2\}$	11.1	13.45	14.4	14.3	12.6	13.8	14.0	12.8
$R_{Bragg} = 100\sum\lvert I_o - I_c\rvert/\sum I_o$	5.45	3.51	3.33	2.94	5.33	5.83	4.49	3.59
Goodness of fit = R_{wp}/R_{exp}	1.49	0.91	0.92	0.88	1.03	1.25	1.01	0.95

[a]Compositional parameter x ($Fe_{4-x}^{3+}Fe_{3x}^{2+}(PO_4)_3(OH)_{3-3x}O_{3x}$) determined by projecting the representing points of the compositions (column 2) in the anhydrous system FeO–Fe_2O_3–P_2O_5 onto the pseudo binary tieline between $Fe_2(PO_4)O$ and $Fe_4(PO_4)_3(OH)_3$.

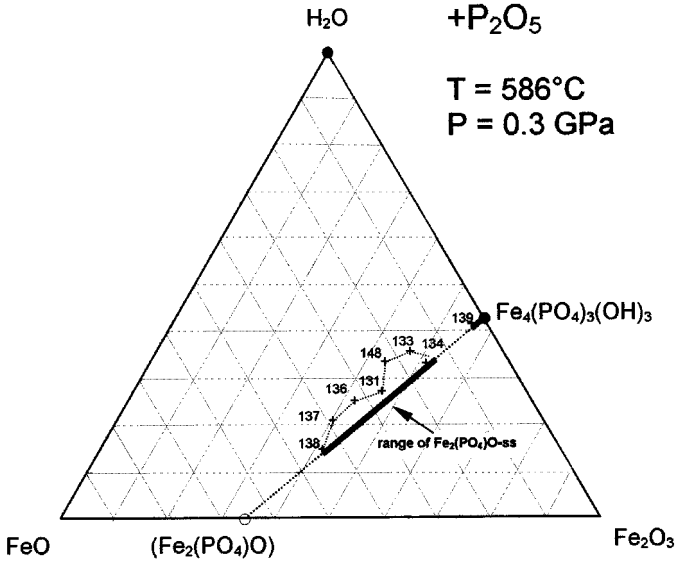

FIG. 6. The system Fe_2O_3–FeO–P_2O_5–H_2O projected from the P_2O_5 apex onto the Fe_2O_3–FeO–H_2O base at 586°C and 0.3 GPa. Crosses: compositions of the $Fe_2(PO_4)O_{ss}$.

of the capsules, the sample size, and the run duration. In the case of reduction the representing data point of the solids of a sample with a starting bulk composition of Fe_2PO_4O would move in the ternary system FeO–Fe_2O_3–P_2O_5 and reach the tieline between Fe_2O_3 and $Fe_3(PO_4)_2$ at a composition of $\frac{1}{2}Fe_2O_3 + Fe_3(PO_4)_2$ according to the reaction

$$2Fe_2PO_4O \Rightarrow \tfrac{1}{2}Fe_2O_3 + Fe_3(PO_4)_2 + 1/4O_2. \quad [2]$$

In this case 50 at.% of the ferric iron was reduced. A comparable but lesser effect can also be recognized in samples of this investigation. In disagreement with its ferric starting composition sample Barb-139 ($x_{start} = 0.0$) was found to contain 1.25% (by weight) of FeO after the experiment (Table 3). Therefore only 2.5 at.% of the ferric iron was reduced. The reason for the sample being only slightly reduced during the experiment may be the short run duration of 1 day and the sample size of about 450 mg. The ferrous iron content of this sample, in which besides monoclinic $Fe_4(PO_4)_3(OH)_3$ no other phase could be detected by X-ray diffraction, can be interpreted as due to a small miscibility region in direction to the intermediate $Fe_2(PO_4)O$ solid solution series.

Lattice Parameters of the $Fe_2(PO_4)O_{ss}$ Members

Figure 7 shows the Rietveld plot of a member of the $Fe_2PO_4O_{ss}$ solid solution series with $x_{exp} = 0.35$ as an

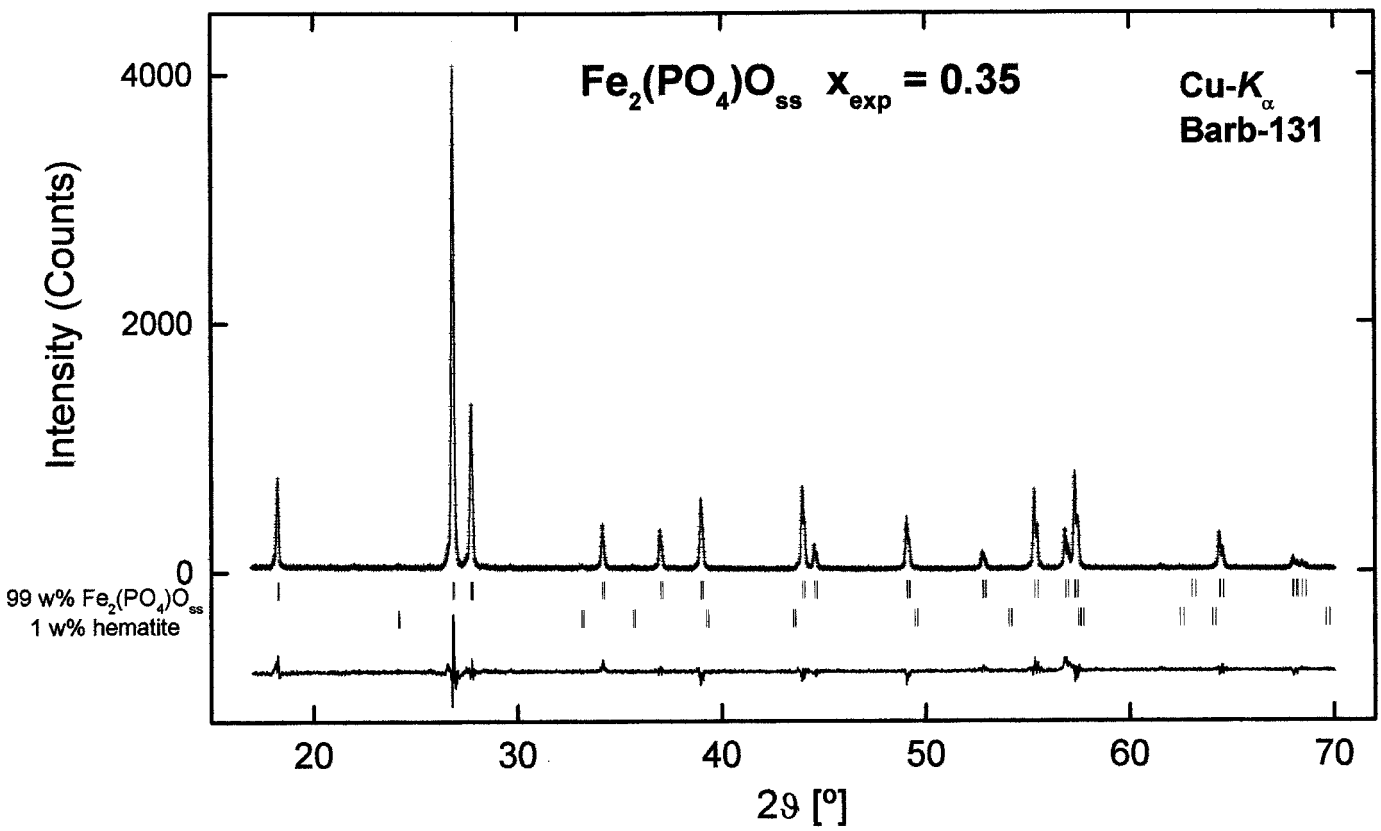

FIG. 7. Observed, calculated, and difference XRPD patterns (Cu$K\alpha$ radiation) of the member of the $Fe_2(PO_4)O_{ss}$ solid solution with $x_{exp} = 0.35$ (sample Barb-131).

example. The sample is composed of a nearly pure solid solution member with about 1% (by weight) of α-Fe_2O_3 (hematite) as an impurity phase (Table 2). The X-ray powder diffractograms were refined starting with the structural data of β-Fe_2PO_4O given by (7) (space group $I4_1/amd$). As no additional reflections with the exception of those belonging to the identified impurity phases like hematite were detected, this space group was taken as appropriate to describe the symmetry properties of the members of the $Fe_2PO_4O_{ss}$ solid solution series when standard X-ray powder diffractometry is used.

The results of the lattice constants refinement are shown in Fig. 8 with literature data of β-Fe_2PO_4O (7). The lattice parameters a, c and the volume of the unit cell V change continuously with composition within the range of the intermediate solid solution series between $0.18 \leq x_{exp} \leq 0.60$. Whereas the unit cell parameter a and the volume of the unit cell V increase the parameter c decreases with increasing x. In Fig. 8c a linear fit to the volume data of the intermediate solid solutions is included which was extrapolated to the compositional region of β-Fe_2PO_4O. This procedure results in an extrapolated volume of $V_{ext}(\beta$-

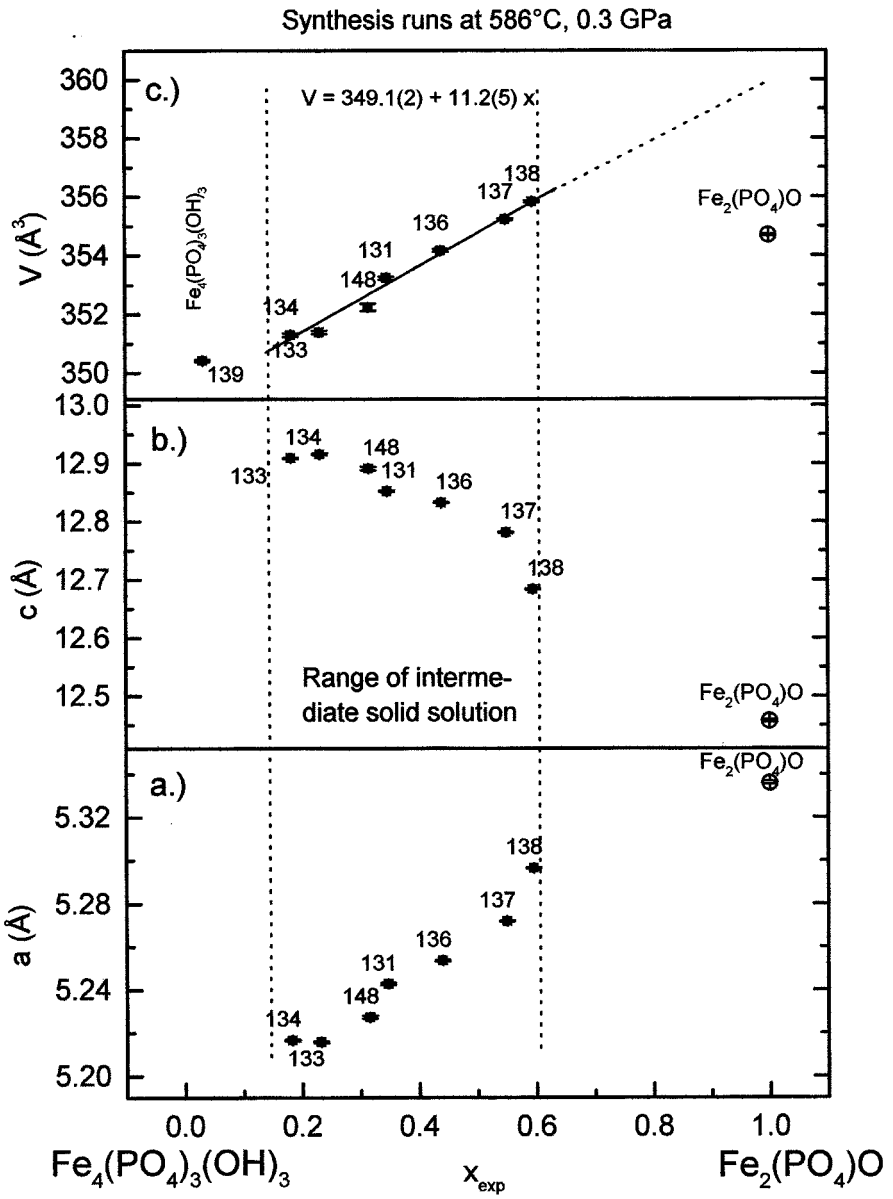

FIG. 8. Lattice parameters a, c and volume of the unit cell V of members of the $Fe_2(PO_4)O$ solid solution series synthesized at 586°C and 0.3 GPa vs composition (full squares). Open circle: data for β-$Fe_2(PO_4)O$ from (7).

Fe_2PO_4O) = 360 Å^3 which is significantly greater than the experimental value of $V = 354.7$ Å^3 given by (7). β-Fe_2PO_4O prepared by (7) was synthesized at 450°C in an H_2–H_2O atmosphere and then recrystallized at 600°C in an evacuated silica tube in the presence of 2% (by weight) of $FeCl_2$. At higher temperatures an irreversible and reconstructive phase transformation to α-$Fe_2(PO_4)O$ was reported (7). The lower volume of the unit cell V given by these authors for β-$Fe_2(PO_4)O$ may be an indication that this compound is stable only at high pressures.

In catalytic studies synthetic barbosalite and lipscombite (both $Fe_3(PO_4)_2(OH)_2$) as well as $Fe_5(PO_4)_3O_3$ and $Fe_{4.24}(PO_4)_3(OH)_{2.20}O_{0.72}$ were transformed during catalysis into members of the $Fe_2(PO_4)O_{ss}$ solid solution series by oxidation and dehydration (3). For synthetic barbosalite this process can be described by the reaction

$$4Fe^{2+}Fe_2^{3+}(PO_4)_2(OH)_2 + \tfrac{1}{2}O_2 \Rightarrow 2Fe_2(PO_4)O + 2Fe_4(PO_4)_3(OH)_3 + H_2O. \quad [3]$$

In Eq. [3] Fe_2PO_4O and $Fe_4(PO_4)_3(OH)_3$ have to be regarded as components of a distinct member of the $Fe_2PO_4O_{ss}$ solid solution series with $x = 0.25$ according to the formula $Fe_{4-x}^{3+}Fe_{3x}^{2+}(PO_4)_3(OH)_{3-3x}O_{3x}$. Analogously for the oxidation and dehydration products of

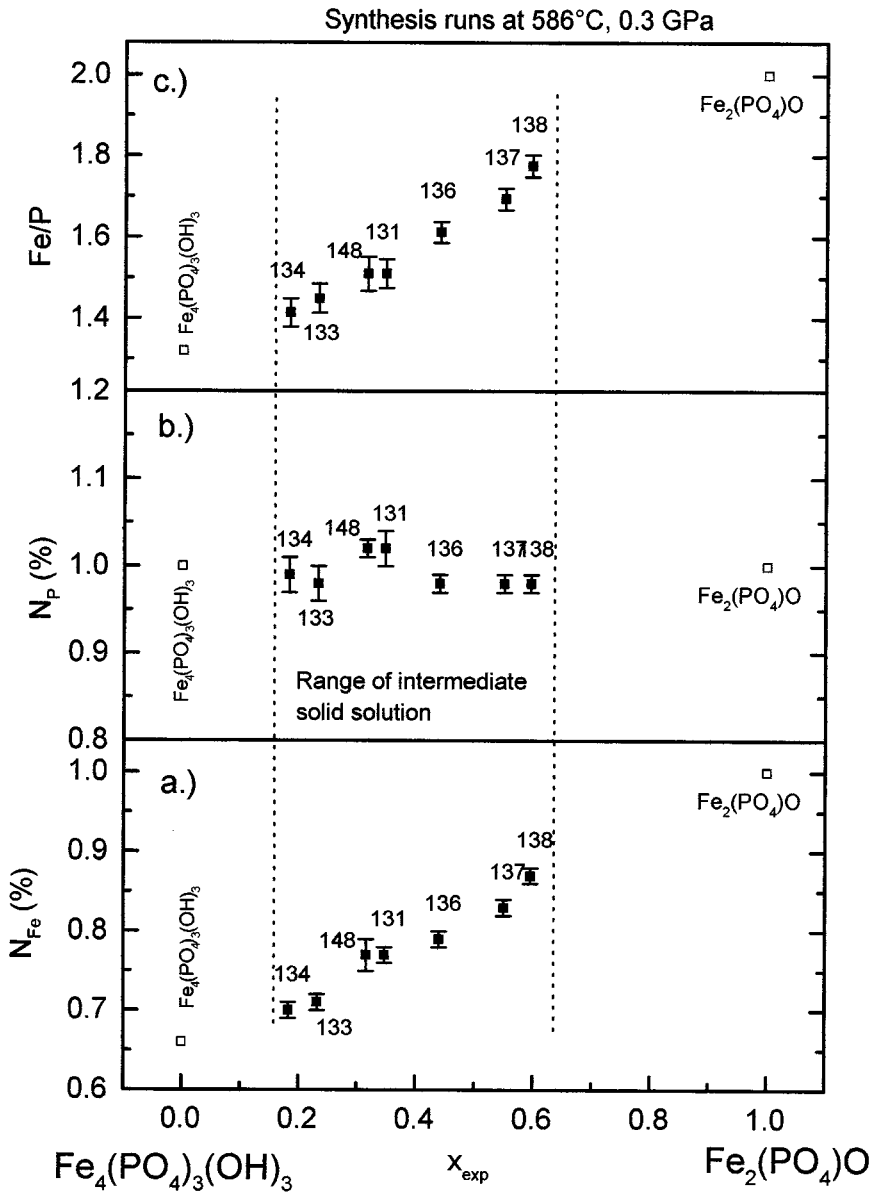

FIG. 9. Site occupancy fractions of (a) the iron site, (b) the phosphorus site, and (c) the Fe/P ratio vs composition. Data from the Rietveld refinement of the members the $Fe_2(PO_4)O_{ss}$ solid solution series (full squares) taken from Table 5. Open squares: data for β-$Fe_2(PO_4)O$ (7) and $Fe_4^{3+}(OH)_3(PO_4)$ (8,9).

$Fe_{4.24}(PO_4)_3(OH)_{2.20}O_{0.72}$ and $Fe_5(PO_4)_3O$ x values of $x = 0.12$ and $x = 0.50$ result. As can be seen in Fig. 8 the x values of $Fe^{2+}Fe_3^{3+}(PO_4)_2(OH)_2$ and $Fe_5(PO_4)_3O$ after catalysis (3) fit into the range of the solid solution whereas the x value of $Fe_{4.24}(PO_4)_3(OH)_{2.28}O_{0.72}$ is located near to its lower limit but within the two-phase field near the $Fe_4(PO_4)_3(OH)_3$ composition. Unfortunately, Rouzies *et al.* (3) did not give any lattice or structural data for their iron hydroxy phosphates after catalysis. But an inspection of the diffractograms given by these authors (Fig. 5 of Ref. (3)) reveals a strong resemblance between their diffractions and those of the members of the $Fe_2(PO)_4O_{ss}$ solid solutions series investigated here (Fig. 4).

Structural Properties of the $Fe_2(PO_4)O_{ss}$ Members

Figure 9 shows the site occupancy fractions (SOF) of iron and phosphorus in the tetragonal structure of the $Fe_2(PO_4)O_{ss}$ solid solutions series in comparison to β-$Fe_2(PO_4)O_{ss}$ and $Fe_4(PO_4)_3(OH)_3$. In the case of the monoclinic compound $Fe_4(PO_4)_3(OH)_3$ the occupancy of the iron site was averaged over the four symmetrically different octahedra for better comparison.

While the data for phosphorus scatter around the value typical for full site occupancy (SOF = 1) the occupancy fraction of the Fe position as well as the Fe/P ratio increase continuously with increasing x in the range of the intermediate solid solution series. This indicates a continuously increasing occupancy of the Fe ($8f$) cation site when going from $Fe_4(PO_4)_3(OH)_3$ toward the $Fe_2(PO_4)O$ composition.

In order to give a geometrical explanation for the contrary behavior of the a and c unit cell parameters (Figs. 8a and 8b) structural properties like the Fe–Fe distance, the Fe–O2 bond length, and the tilting angle ϕ between neighbouring FeO_6 octahedra were calculated and plotted in Fig. 10. According to the arrangement of the structure in space group $I4_1/amd$ the infinite chains of face-sharing oxygen octahedra are oriented parallel to the [100] and the [010] directions (Fig. 11). These octahedra are symmetrically equivalent and are occupied by disordered Fe^{2+} ions, Fe^{3+} ions, and vacancies. The distance between two neighboring Fe sites, d(Fe–Fe), equals half the lattice parameter a. The oxygen octahedra are built up of two different types of oxygen ions, O1 and O2, respectively. As the O2–Fe–O2 bond angle equals 180°, the lattice constant c can be expressed using the d(Fe–O2) and the d(Fe–Fe) bond lengths as

$$c = 8\sqrt{d_{\text{Fe-O2}}^2 - (d_{\text{Fe-Fe}}/2)^2}, \quad c, d \text{ in Å} \qquad [4]$$

According to Figs. 10a and 10b with increasing x and therefore increasing occupancy of the Fe site the Fe–Fe distance grows (which can be explained by an increased repulsion between the Fe sites) and simultaneously the

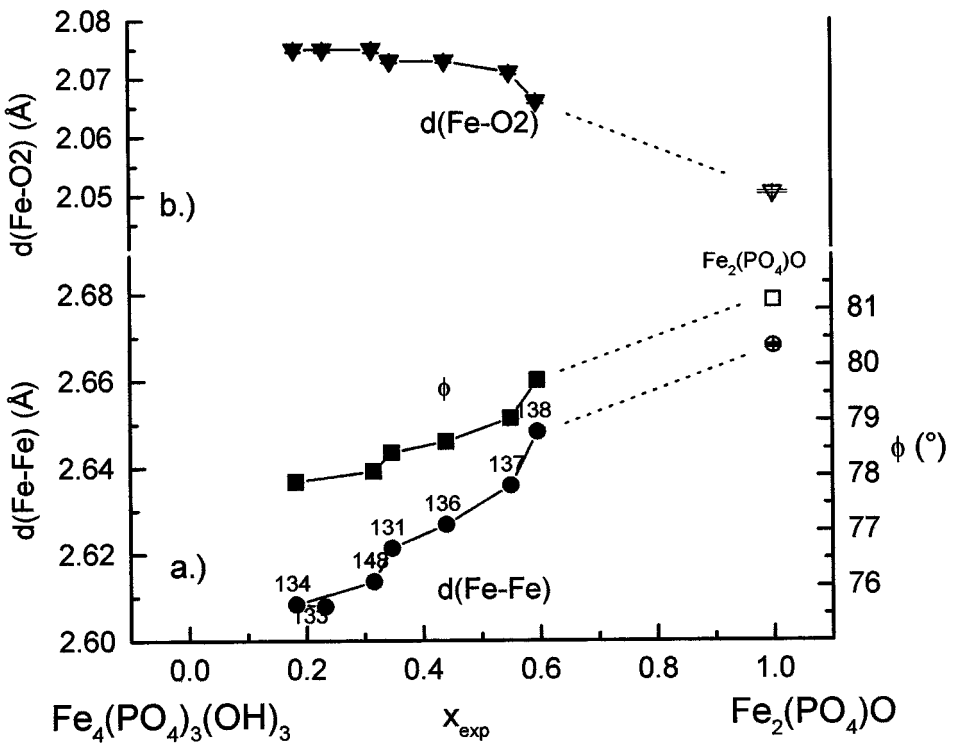

FIG. 10. Fe–Fe distance, Fe–O2 bond length, and tilting angle φ between neighboring Fe–O_6 octahedra in the tetragonal structure of members of the $Fe_2(PO_4)O_{ss}$ solid solution series.

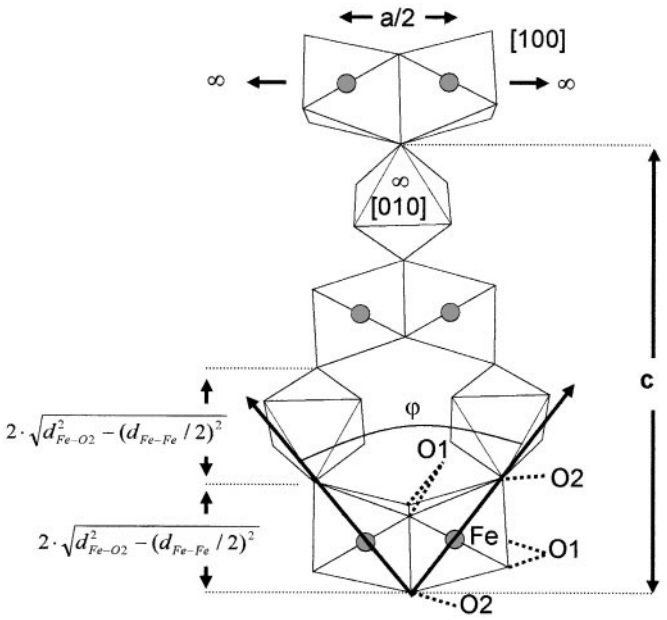

FIG. 11. Geometrical relationship between the Fe–Fe distance, Fe–O2 bond length, and the lattice constants in members of the $Fe_2(PO_4)O_{ss}$ solid solution series. Shaded circles: Fe (8*f*) site, partially occupied by Fe^{3+}, Fe^{2+}, and vacancies.

Fe–O2 bond length decreases. According to Eq. [4] the variations of these changes in *d*(Fe–Fe) and *d*(Fe–O2) are responsible for the observed reduction of the *c* lattice parameter with increasing $Fe_2(PO_4)O$ content of the solid solutions. As a consequence the undulated chains of oxygen octahedra (see Figs. 2a and 11) are then elongated and flattened as the tilting angle ϕ of neighboring octahedra is increased (Fig. 10).

CONCLUSIONS

In contrast to previous investigations (7) it was found that an intermediate solid solution series between the representing points of the $Fe_2(PO_4)O$ and $Fe_4(PO_4)_3(OH)_3$ compositions in the quaternary system $FeO–Fe_2O_3–P_2O_5–H_2O$ can be synthesized under hydrothermal conditions. Using standard X-ray powder diffraction, these compounds were found to crystallize in the space group $I4_1/amd$. The Fe^{3+} ions, Fe^{2+} ions, and vacancies are therefore disordered over the symmetrically equivalent octahedral (8*f*) sites. At this state of the investigation a small monoclinic distortion of the structure analogous to the observations (10) concerning β-$Fe_2(PO_4)O$ cannot be ruled out. To investigate quantitatively the presence of any deviations from a disordered distribution of ferrous and ferric iron as well as the octahedral vacancies, a more detailed single-crystal study using synchroton radiation and/or electron diffraction might be necessary.

ACKNOWLEDGMENTS

The author thanks Dr. Frederic Hatert and Mr. J.-M. Speetjens (University of Liège, Belgium) for the chemical analysis of the samples and Prof. L. Cemič (University of Kiel, Germany) for critical reading of the manuscript.

REFERENCES

1. E. Cavatera, *U. S. Patent 3 948 959*, Montedison, 1976.
2. C. Daniel, *U. S. Patent 4 298 755*, Ashland Oil Inc., 1981.
3. D. Rouzies, J. M. M. Millet, D. S. H. Sam, and J. C. Védrine, *Appl. Catal. A*: *General* **124,** 189–203 (1995).
4. E. Muneyama, A. Kunishige, K. Ohdan, and M. Ai, *Bull. Chem. Soc. Jpn.* **69,** 509–513 (1996).
5. J. M. M. Millet, *Catal. Rev.-Sci. Eng.* **40**(1&2), 1–38 (1998).
6. B. Ech-Chahed, F. Jeannot, B. Malaman, and C. Gleitzer, *J. Solid State Chem.* **74,** 47–59 (1988).
7. M. Ijjaali, B. Malaman, C. Gleitzer, K. Warner, J. A. Hriljac, and K. Cheetham, *J. Solid State Chem.* **86,** 195–205 (1990).
8. C. C. Torardi, W. M. Reiff, and L. Takaks, *J. Solid State Chem.* **82,** 203–215 (1989).
9. M. Ijjaali, B. Malaman, C. Gleitzer, and M. Pichavant, *Eur. J. Solid State Inorg. Chem.* **26,** 73–89 (1989).
10. E. Elkaïm, J. F. Berar, C. Gleitzer, B. Malaman, M. Ijjaali, and C. Lecomte, *Acta Crystallogr. B* **52,** 428–431 (1996).
11. H. Ungethüm, *Z. Angew. Geol.* **11** (9), 500–505 (1965).
12. J. S. Huebner, *in* "Research Techniques for High Temperature and High Pressure" (G. C. Ulmer, Ed.), pp. 123–177. Springer Verlag, Berlin, 1971.
13. D. Rouzies and J. M. M. Millet, *Hyperfine Interactions* **77,** 11–18 (1993).